Geolocation and Pointing Accuracy Analysis for the WindSat Sensor

William E. Purdy, Peter W. Gaiser, *Senior Member, IEEE*, Gene A. Poe, *Member, IEEE*, Enzo A. Uliana, Thomas Meissner, and Frank J. Wentz

***Abstract*—Geolocation and pointing accuracy analyses of the WindSat flight data are presented. The two topics were intertwined in the flight data analysis and will be addressed together. WindSat has no unusual geolocation requirements relative to other sensors, but its beam pointing knowledge accuracy is especially critical to support accurate polarimetric radiometry. Pointing accuracy was improved and verified using geolocation analysis in conjunction with scan bias analysis. Two methods were needed to properly identify and differentiate between data time tagging and pointing knowledge errors. Matchups comparing coastlines indicated in imagery data with their known geographic locations were used to identify geolocation errors. These coastline matchups showed possible pointing errors with ambiguities as to the true source of the errors. Scan bias analysis of U, the third Stokes parameter, and of vertical and horizontal polarizations provided measurement of pointing offsets resolving ambiguities in the coastline matchup analysis. Several geolocation and pointing bias sources were incrementally eliminated resulting in pointing knowledge and geolocation accuracy that met all design requirements.**

***Index Terms*—Geolocation, polarimetry, radiometry.**

I. Introduction

WINDSAT is a satellite-based multifrequency polarimetric microwave radiometer developed by the Naval Research Laboratory (NRL) for the U.S. Navy and the National Polar-orbiting Operational Environmental Satellite System (NPOESS) Integrated Program Office (IPO) [1]. WindSat is designed to demonstrate the capability of polarimetric microwave radiometry to measure the ocean surface wind vector from space. The sensor provides risk reduction for the development of the Conical Microwave Imager Sounder (CMIS), which is planned to provide wind vector data operationally starting in 2010. WindSat is the primary payload on the Department of Defense Coriolis satellite, which was launched on January 6, 2003. It is in an 840-km circular sun-synchronous orbit. The WindSat receivers are total power radiometers operating in discrete bands at 6.8, 10.7, 18.7, 23.8, and 37.0 GHz. The 10.7-, 18.7-, and 37.0-GHz channels are fully polarimetric, while the 6.8- and 23.8-GHz channels are dual polarized only (vertical and horizontal).

Geolocation of satellite data is a standard part of the postlaunch calibration process. For the data to be of value, it is critical that the measured parameters be correctly mapped to the surface of the Earth. The WindSat geolocation evaluation process closely follows the techniques used for the Special Sensor Microwave/Imager (SSM/I) [2]. Because WindSat is a polarimetric radiometer, knowledge of the pointing errors is also critical. Polarimetric radiometers and the wind direction retrieval are particularly sensitive to pointing errors, thus placing significant emphasis on their removal in the calibration process. Errors in pointing knowledge directly affect the Earth incidence angle (EIA) and the polarization rotation angle (PRA). Knowledge errors in the latter introduce cross-polarization resulting in errors in the Stokes parameters, which causes degradation in the wind vector retrieval and other environmental data records (EDRs). The knowledge requirements driven by geolocation are far less stringent than those driven by pointing. However, the tools used for geolocation also apply to the pointing analysis.

Initial geolocation performance was significantly worse than required because of pointing knowledge and data time tagging errors. The WindSat pointing and geolocation performance improved in several increments ultimately meeting all pointing knowledge and geolocation requirements. This paper will emphasize the challenges in meeting the knowledge requirements and will explain how the analyses revealed the necessary information. Properly identifying and differentiating between timing and pointing errors required two independent analysis methods. Coastline analyses comparing WindSat imagery to coastline maps from the World Vector Shoreline Data Bank II (WVS II) identified geolocation bias errors. The reported accuracy of the WVS II is better than 518 m for 90% of all identified shoreline features [3] However, the source of the error was ambiguous. Scan bias analysis of the third Stokes vector term, U, and the quantity $V - (1/2)H$ provided quantitative assessment of pointing knowledge bias errors and resolved ambiguities in the coastline matchup analysis.

This paper will emphasize the driving goals of the geolocation and pointing accuracy analysis, the two methods used, the errors identified and eliminated, and the ultimate geolocation and pointing knowledge performance of the WindSat instrument. The capabilities, limitations, and complementary nature of the two analytical methods used to improve pointing knowledge will be discussed in detail.

Manuscript received February 23, 2005; revised June 9, 2005.

W. E. Purdy is with Purdy Engineering, Inc., Poolesville, MD 20837 USA.

P. W. Gaiser is with the Naval Research Laboratory, Washington, DC 20375 USA (e-mail: peter.gaiser@nrl.navy.mil).

G. A. Poe is with the Naval Research Laboratory, Monterey, CA 93943 USA.

E. A. Uliana is with Interferometrics, Inc., Chantilly, VA 20151 USA.

T. Meissner and F. J. Wentz are with Remote Sensing Systems, Santa Rosa, CA 95401 USA.

Digital Object Identifier 10.1109/TGRS.2005.858415

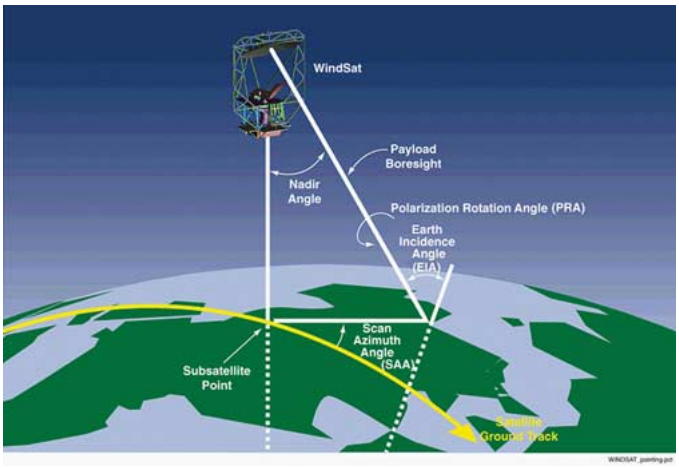

Fig. 1. WindSat pointing definitions.

II. Geolocation Analysis

A. Requirements

The geolocation and pointing analysis had the goal of determining the corrections necessary for the WindSat data to meet the requirements below. Fig. 1 shows the definition of the pointing angles in these requirements.

- Earth incidence angle knowledge bias $\pm 0.05^\circ$. An EIA pointing error, bias or random, of 0.05° would also cause a $\pm$ ~1-km geolocation error. Note that at a 45° nadir angle, 0.05° EIA error is equivalent to 0.036° of pitch error.
- Polarization rotation angle knowledge bias $\pm 0.05^\circ$. A roll pointing error, bias or random, of 0.05° would cause 0.05° PRA and would also cause a $\pm$ ~1-km geolocation error.
- Geolocation accuracy ± 5 km, as specified in the NPOESS Integrated Operational Requirements Document for global ocean surface wind vector.
- Scan azimuth angle (SAA) $\pm 0.25^\circ$. This is driven by the 5-km geolocation requirement.

In addition to spacecraft attitude and GPS data, the antenna beam pointing and data time tagging drive the WindSat geolocation. WindSat uses 11 dual-polarization feedhorn antennas resulting in 22 beams pointed in 11 different directions [1]. Pointing errors may be systematic affecting all 11 beams or may be attributable to individual beams. The antenna alignment and beam pointing were characterized during prelaunch testing [4].

The geolocation accuracy needed for EDR placement (± 5 km) is far less stringent than the geolocation accuracy that results from meeting beam pointing knowledge requirements. The 37-GHz channel has the smallest 3-dB footprint of any WindSat channel at 8×13 km. Thus, achieving the EIA and PRA requirements of 0.05° results in a geolocation accuracy of about $1/8$ of the smallest pixel size or ± 1 km.

B. Geolocation Analysis Technique

All coastline matchups use WindSat antenna temperatures mapped onto the Earth, called temperature data records (TDRs) [1]. This is referred to as imagery data when a swath of sequential data samples is plotted on a map of the Earth creating an image of the antenna temperatures. A variety of definitions of terms used in the geolocation analysis appears in the Appendix.

The coastline analysis method determines the geolocation inaccuracy of the plotted data samples. These inaccuracies are determined in two ways. First, one compares known coastlines to the coastlines apparent in the imagery data. Coastlines appear in the imagery data as dramatic temperature changes at land water boundaries caused by the significant differences in brightness temperatures for land and water. The raw imagery clearly shows coastlines; however, the transition from water to land typically occurs over a blended region approximately 20 km wide. One can visually pick the midpoint of this transition with an accuracy of perhaps 5 km, but this method is nowhere near as accurate as the 1-km accuracy required to determine 0.05° pointing errors.

A second method was developed by NRL prior to the WindSat program which analyzes the imagery data to pick the local maximum temperature gradient along scan and cross scan [5]. Fig. 2 shows imagery data and the corresponding local maxima plots. Taking the partial derivative of the sampled radiometer data with respect to the scan contains information about the antenna gain function in the along-scan direction. In particular, an estimate may be made of the position of the "mean" shoreline in terms of the location associated with the maximum of the partial derivative of the sampled data. Taking advantage of the fact that a cubic spline function provides very smooth interpolation of data (continuous first and second derivatives), we may obtain a smooth first derivative of the radiometer samples with respect to the sample number and solve for the fractional sample number associated with the peak of the derivatives. Using the latitude and longitude coordinates for the sampled data we may then readily convert the fractional sample number to latitude and longitude coordinates associated with the peak of the gain function.

The local maxima procedure may be automated by searching for all maxima in the cubic spline fit satisfying a minimum threshold level for each scan crossing a shoreline. The sample numbers of the resulting peaks may be readily determined and converted to latitude and longitude coordinates. It should be noted that the same procedure may be used in the along-track direction for a fixed along-scan sample. Thus, both along-scan and along-track estimates may be made for those scans that cross shorelines, as plotted in Fig. 2. This map of local maxima represents the coastlines quite well and provides a finer resolution and quantitative representation of a presumed land sea boundary. It will later be shown that this method represents the coastline to an accuracy of less than 2 km.

The geolocation errors for a given swath of data are examined and the offsets between the imagery and local maxima indicated coastline and the known coastline are estimated over the following parameters: forward scan, aft scan, cross scan, along scan for each radiometer channel. Careful study of the characteristics of these errors provides important clues about the source of the error. The effect of each type of pointing and timing error on the geolocation is included in the definition of these terms in the Appendix. The nature of the error, bias or random, is determined by the consistency, or lack thereof, in these errors.

In heritage systems such as SSM/I, determination of error sources was of secondary importance so long as the data were geolocated to within the required accuracy. The required polarization accuracy forces tighter pointing knowledge requirements for polarimetric radiometers such as WindSat.

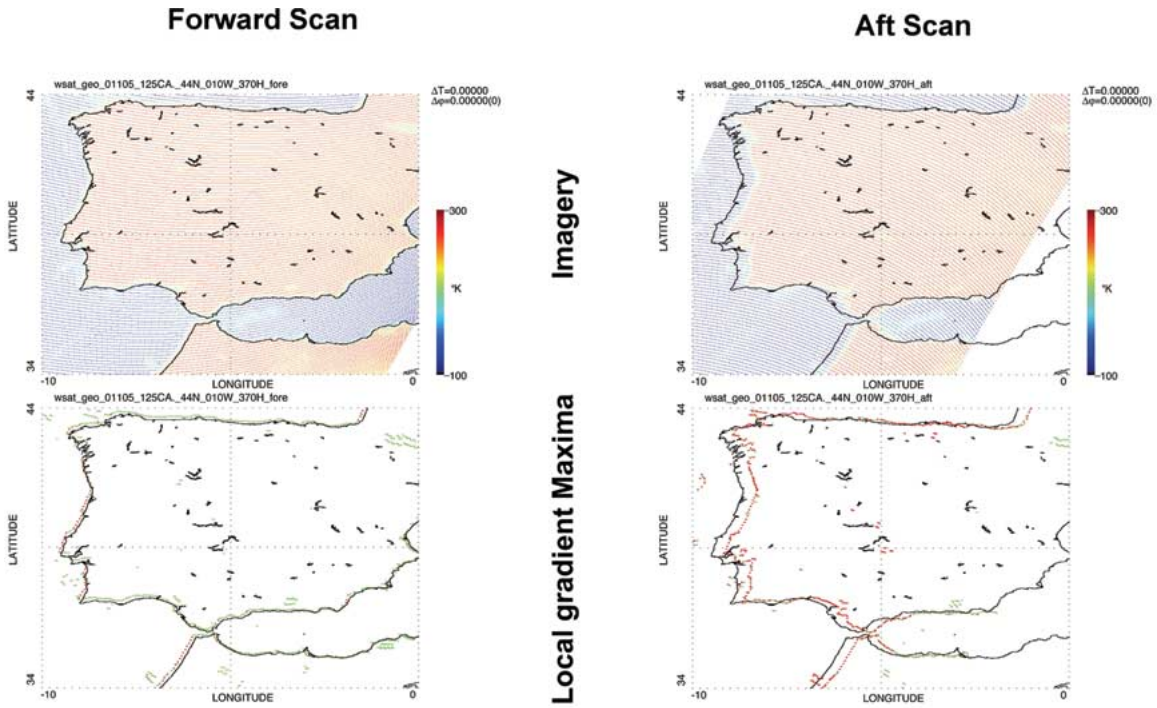

Fig. 2. Imagery data and corresponding local maxima plots. Data from rev 1105, a descending pass, over Spain with geolocation errors resulting from initial processing errors. These datasets are analyzed visually to extract the coastline matchup results. The green dots in the local maxima plots represent cross-scan local maxima, while the red dots indicate along-scan local maxima.

Thus resolving the cause of an error becomes necessary to understanding whether the pointing is affected.

The approach taken in the WindSat program was to calculate the sensor error necessary to create a given set of geolocation errors. This calculation assumes that all geolocation error in a given direction, e.g., north, is caused by a single sensor error source. For example, if all of the coastline data appear 10 km north of the geographic coastline in the forward and aft scan of an ascending pass then it can be calculated from orbital parameters that a systematic timing bias of 1.35 s could have caused this geolocation error. However, it can also be shown that this same set of 10-km errors could result from a 0.26° upward pitch bias knowledge error. This example highlights the ambiguity of error sources, which is one of the largest challenges in geolocation/pointing analysis.

In the same way that one can calculate pitch and systematic timing errors in the above example one can calculate the geolocation effects from all other possible sensor errors. Table I shows how each sensor error affects the coastline matchups. One can determine most of the sensor error behavior by using the properties in the table. The inherent ambiguities, noted in the table, often limit final identification of the error source. For example, pitch errors can be separated from beam azimuth and elevation, roll, yaw, and within scan timing, but pitch cannot be separated from systematic timing errors. Within scan timing error is a form of timing error unique to the WindSat payload in that a time tagging error builds incrementally around a single scan and is reset to zero error at the start of each subsequent scan. Within scan timing errors are explained in more detail in the Appendix. The concept of this table can also be applied to sensors with a single forward scan as certain errors will have different effects at beginning and end of scan.

TABLE I
TRUTH TABLE RELATING SENSOR ERRORS TO GEOLOCATION ERRORS

ASCENDING PASS.
ALL VALUES REVERSE FOR DESCENDING PASS

	FORWARD SCAN EFFECT	AFT SCAN EFFECT	ALL CHANNELS?	AMBIGUITY?	COMMENTS
POSITIVE ROLL	WEST	WEST	YES	ERRORS IN ANY 2 PRODUCE AMBIGUITIES FOR ALL (EXCEPT YAW & BEAM AZ)	VALUES REVERSE FOR NEG ROLL
POS YAW	ALONG SCAN TO WEST	ALONG SCAN TO EAST	YES		VALUES REVERSE FOR NEG YAW
POSITIVE BEAM AZIMUTH	ALONG SCAN TO WEST	ALONG SCAN TO EAST	NO		VALUES REVERSE FOR NEG AZ
WITHIN SCAN TIMING ERROR	SMALL ALONG SCAN TO WEST	LARGER ALONG SCAN TO EAST	NO		CONSISTENT WITHIN A GIVEN FREQ BAND
POSITIVE PITCH	SOUTH	SOUTH	YES	AMBIGUITY	VALUES REVERSE FOR NEG PITCH
POSITIVE SYSTEMATIC TIMING ERROR	SOUTH	SOUTH	YES		VALUES REVERSE FOR NEG TIMING
POSITIVE ELEVATION	CROSS SCAN TO NORTH	CROSS SCAN TO SOUTH	NO		VALUES REVERSE FOR NEG ELEV

Analyzing geolocation performance involved studying several datasets for several channels. A dataset would be selected over a 10° latitude by 10° longitude area that had a good variety of north/south and east/west coastlines; Spain, Tasmania, the Yucatan peninsula, and the gulf between Argentina and Uruguay proved especially useful. Island groups were also considered, but the high spatial variability of the island shorelines usually added uncertainty to the analysis. The raw imagery and gradient maps were produced for all 22 WindSat channels for one or more datasets. All of these datasets were then analyzed. It was found that all channels within a frequency band had identical geolocation performance; however geolocation would vary between frequency bands. Once this in-band consistency was confirmed, only the vertical and horizontal channels for each frequency band were plotted for the remaining datasets with differing geographic locations and a roughly equal number of ascending and descending passes. The results from the total of

five to ten datasets, depending on geolocation site, were averaged by channel and the results studied. Estimated errors varied by roughly 25% from rev to rev, primarily because of the visual and judgmental nature of determining geolocation from the imagery maps. Five to ten datasets were sufficient to average out this inconsistency. The relative consistency of the datasets and the small amount of averaging required indicates that the errors were primarily driven by biases. While more averaging would generally be more accurate, the error reduction needs did not call for this level of resolution.

III. Incremental Elimination of Geolocation

Several WindSat pointing and timing errors were incrementally eliminated by a combination of the coastline matchup method and a scan bias analysis. The initial sets of WindSat imagery showed significant geolocation errors resulting from the sensor data and the processing.

A key requirement for eliminating errors is to properly identify the error source. If one fixes an error stemming from poor time tagging with a pointing correction, the data will then be geolocated properly, but will have the original timing errors and have erroneously inserted pointing errors that degrade the wind retrievals.

Geolocation maps and accuracy results will be shown in figures for each incremental step. These figures each show an extreme close-up (approximate $3^\circ \times 3^\circ$ latitude/longitude box) of local maxima data for the 37 H channel from rev 1105, a descending pass over Gibraltar. Each figure also includes a table of the pitch, roll, and within-scan timing errors. These calculations assume that all geolocation error in a given direction, e.g., north, is caused by a single sensor error source. To demonstrate the effects of each stage of error reduction, the figures show data from this same rev (1105) but reprocessed to remove the relevant pointing or timing error.

A. First Increment: Initial Data

The initial dataset had geolocation errors ranging from 3–12 km in both forward and aft scans and in both east/west and north/south orientations. Several orbits, or revs, of data were analyzed and the results were averaged for each possible sensor error. Fig. 3 presents the results for pitch, roll and within scan timing errors, and the coastline matchups. All 22 channels had the same general skewing showing us that the largest problems were systematic rather than isolated to individual channels. The geolocation imagery clearly shows larger errors in the aft scan than in the forward scan.

All the data are generally skewed to the north for descending passes (such as 1105) and to the south for ascending passes, which is indicative of either a pitch or systematic timing error. We judged that a pitch bias of 0.27° was unlikely given the accuracy with which the payload was built and measured; thus, we suspected a systematic timing bias. Manually introducing timing corrections in postprocessing of the imagery data confirmed that a systematic timing offset of 1.92 s would create the effect observed. Discussions among sensor, spacecraft, and ground software engineers identified an exact 1-s timing error resulting from mishandling the GPS time tagging in the WindSat ground data processing software (GDPS). Modification of the WindSat GDPS corrected this now-known timing bias.

For this descending pass the forward data are skewed to the west, while the aft data are skewed to the east, with this skewing inverted in ascending passes. It appears that the along scan error is increasing with progression around the scan. This behavior suggests an error in how individual radiometer samples are time-tagged, referred to as a within-scan timing error (Appendix). This effect would explain much of the large aft easterly error. Simulating the effect in postprocessing of imagery data produced an estimate of the timing error. An additional delta time of 5.28 μs was added to each sample around the scan according to the equations in Fig. 8. This change greatly improved the geolocation. Discussions with the sensor and GDPS engineers revealed that the GDPS did not account for five cycles of the WindSat master clock (921.6 kHz or 1.085 μs/cycle) in the sensor time tagging. This error was corrected in the ground processing software.

The geolocation analysis tool can be used to quickly converge on likely error sources by manually inserting theorized error corrections in postprocessing of the data. This was done in both cases above to identify suspicions that the timing had significant errors. Theorized pointing as well as timing errors can be inserted. This is especially valuable when one suspects that there is more than one error source.

The initial increment of geolocation analysis had identified two proven time-tagging errors, which were corrected. A thorough review of all time tagging throughout the sensor and spacecraft and ground processing was performed and did not uncover any additional errors.

B. Second Increment: Incorporation of Corrected Timing

The second phase increment analyzed coastline matchups of several revs of data with the known timing errors fixed. Fig. 4 shows the averaged results and representative imagery. The imagery, while showing dramatic improvement in the aft scan, still contains errors. These errors were consistent throughout many datasets indicating that they were the result of biases not yet removed. The quantitative errors in the table of Fig. 4 suggest that the errors are consistent across all channels; therefore, they likely have systematic sources. The geolocation accuracy was 3–5 km, which meets the 5-km requirement. If the remaining biases were all due to pointing, they would be on the order of 0.12° for both pitch and roll, exceeding the sensor design pointing error budget. These magnitudes are more than twice the 0.05° bias specified in the error budget, but are within the range of credible build and test errors.

The biases remaining to be eliminated now represented subpixel geolocation accuracy. A key aspect of the method of calculating local temperature gradient maxima is that it is not tied to pixel size and is thus potentially capable of subpixel geolocation analysis.

Using the coastline analysis, we could not resolve whether the errors stemmed from a pitch offset, a systematic timing bias, or a combination of the two. The beam elevation errors were unambiguously determined to be virtually nil. The aft east/west errors were larger than those in the fore scan. This could be the result of additional within-scan timing errors, roll, yaw, or beam

FIRST INCREMENT: INITIAL GEOLOCATION PERFORMANCE

	AVG PITCH (deg)	AVG ROLL (deg)	AVG WITHIN SCAN (uSEC)	AVG YAW / BEAM AZIMUTH (DEG)
10.7 VH	0.42	0.08	-3.3	0.12
18.7 VH	0.34	0.22	-5.4	-0.28
23.8 VH	0.23	0.37	-6.7	-0.64
37 VH	0.31	0.39	-4.8	-0.84
4 CHANNEL AVERAGE	**0.27**	**0.18**	**-5.1**	**-0.41**
ERROR DIAGNOSIS	LARGE PITCH AND / OR SYSTEMATIC TIMING ERROR	LARGE ROLL AND / OR YAW AND / OR WITHIN SCAN TIMING ERROR		

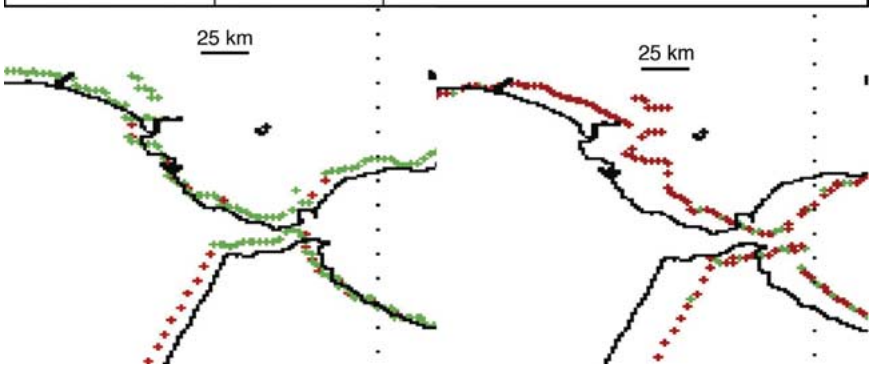

Fig. 3. Geolocation performance in first increment. The table summarizes the average error for several datasets taken from various geographic locations with various pass geometries. The images show a close-up image of local maxima in an area slightly smaller than 3° latitude × 3° longitude. The green dots in the local maxima plots represent cross-scan local maxima, while the red dots indicate along scan-local maxima. (Left) Forward scan. (Right) Aft scan.

SECOND INCREMENT: ALL KNOWN TIMING ERRORS REMOVED

	AVG PITCH (deg)	AVG ROLL (deg)	AVG WITHIN SCAN (uSEC)	AVG YAW / BEAM AZIMUTH (DEG)
10.7	0.10	0.09	-0.18	-0.06
18.7	0.11	0.10	-0.20	-0.06
23.8	0.15	0.18	-0.35	-0.26
37	0.13	0.11	-0.21	-0.14
4 CHANNEL AVERAGE	**0.12**	**0.11**	**-0.23**	**-0.13**
ERROR DIAGNOSIS	LOOKS LIKE PITCH ERROR BUT COULD BE UNDETERMINED SYSTEMATIC TIMING	ROLL / WITHIN SCAN ERRORS / YAW REDUCED BUT CANNOT DETERMINE SOURCE OF REMAINING ROLL OR WITHIN SCAN TIMING ERROR		

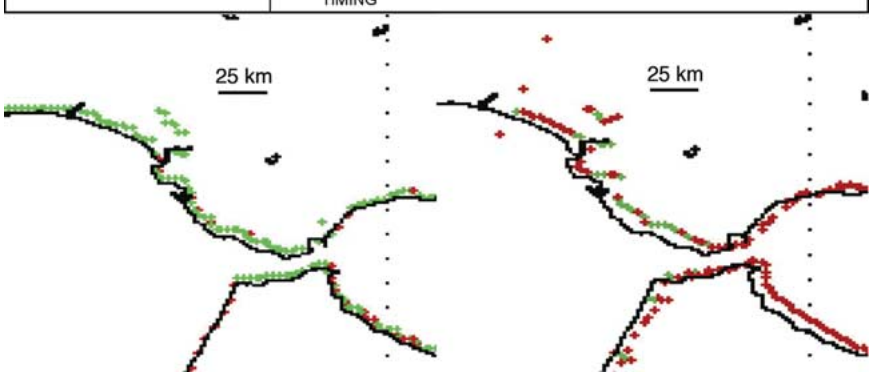

Fig. 4. Geolocation performance in second increment. The table summarizes the average error for several datasets taken from various geographic locations with various pass geometries. The images show a close-up image of local maxima in an area slightly smaller than 3° latitude × 3° longitude. The green dots in the local maxima plots represent cross-scan local maxima, while the red dots indicate along-scan local maxima. (Left) Forward scan. (Right) Aft scan.

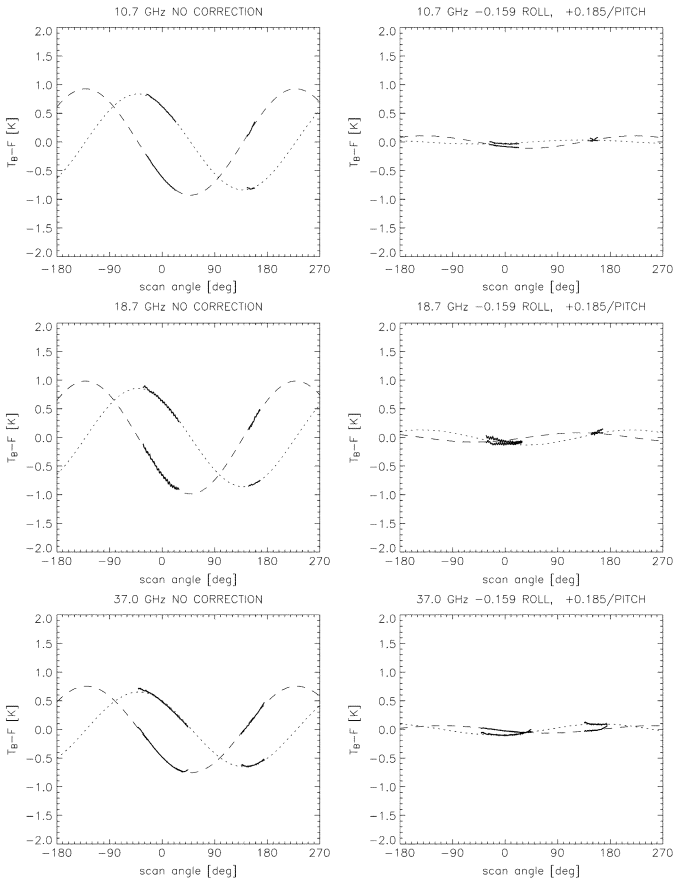

Fig. 5. Along-scan biases. Difference between measured and computed ocean brightness temperatures (in Kelvin) for the combination (dotted line) $V-(1/2)H$ and (dashed line) the third Stokes parameter as a function of the antenna boresight looking azimuth (scan angle) at 10.7, 18.7, and 37.0 GHz. The full segments indicate the scan positions with actual measurements. The dotted and dashed curves are fits to a sinusoidal function. The plot averages orbits rev numbers 3600–4600. The left panel shows the results from the WindSat TDR set [8]. The right panel after the roll/pitch error has been corrected.

azimuth biases, or combinations of any two. While educated assumptions could be made about the probability of the possible error sources, additional analysis tools were needed to quantitatively resolve the ambiguities. The scan bias analysis described next proved to be a powerful tool to identify the source of the remaining errors.

C. Scan Bias Analysis

1) Along-Scan Biases: In our analysis of the WindSat third Stokes parameter U and polarization rotation we examined along-scan biases in the brightness temperatures [6]. The left panel of Fig. 5 shows the difference between the WindSat brightness temperature T_B and a radiative transfer model (RTM) function F for ocean observations [7]. The results shown are an average over WindSat orbits 3600 through 4600 (approximately 2.5 months) and are plotted as a function of the antenna boresight azimuth (scan angle) ω. Averages are done at the three fully polarimetric bands (10, 18, and 37 GHz), and for each band we show the polarization combination $V-(1/2)H$ and the third Stokes parameter U. Because small errors in the atmospheric parameters (columnar water vapor and columnar liquid cloud water) or the atmospheric part of the RTM can introduce a large error in V and H, we are using the difference $V-(1/2)H$ rather than vertical polarization (V-pol) and horizontal polarization (H-pol) themselves, as this combination is much less sensitive to atmospheric uncertainties. The reason for this is that, at the incidence angles and frequencies under consideration, the reflectivity of the ocean surface is about twice as large for H-pol than for V-pol, and therefore atmospheric fluctuations in the brightness temperatures tend to cancel out when taking $V-(1/2)H$.

Large parts of the scan are reserved for calibration and hence do not contain Earth observations but rather hot and cold calibration counts. In order to avoid any roll off in the brightness temperatures that occurs in the vicinity of the calibration targets, we only used observations well away from the calibration zones. The two segments in Fig. 5 indicate the scan positions where Earth measurements were taken during the forward look and the aft look. The larger segment corresponds to the forward look and the smaller segment to the aft look. We have fitted a sinusoidal function (dotted for $V-(1/2)H$ and dashed for U) of the form $A_0+A_1\sin(\omega-\omega_0)$ to each curve. The overall shifts A_0 are of no importance for the present analysis. They result from calibration errors that are independent on the along-scan position such as errors in the reported spillover η or errors in the RTM. This absolute offset will be handled at a later point when performing a full calibration of the WindSat brightness temperatures.

The scan bias analysis produced the following results. For all three polarimetric bands we found substantial biases in the magnitude of 0.5–1.0 K for $V-(1/2)H$ and U within both forward and aft look. In addition, all three polarimetric bands exhibited large oscillations of magnitude 1.0–1.5 K for $V-(1/2)H$ and U between forward and aft look. The oscillation of $V-(1/2)H$ and U have a relative phase of 90° in each band. The sign and phase angle ω_o s approximately the same for all three bands. The amplitude A_1 of the sinusoidal form differs between the three bands. Though not shown here, the two nonpolarimetric bands (7 and 23 GHz) display the same oscillation of $V-(1/2)H$ as shown in Fig. 5. As confirmation, we obtained essentially the same results when performing the same analysis on a different set of orbits. An error in V-pol and H-pol and the third Stokes parameter of this size would pose a very serious problem for any algorithm that tries to retrieve sea surface temperature or sea surface wind speed and direction. It is therefore necessary to find a reliable way to correct these biases.

2) Earth Incidence Angle and Polarization Rotation Angle Errors: The observed along-scan biases in $V-(1/2)H$ and U can be explained by errors in the EIA θ and polarization rotation angle φ that were reported in the WindSat TDR set [8]. A difference $\Delta\theta=\theta_{\rm true}-\theta_{\rm rep}$ leads to an along-scan scan bias

$$\Delta\left(T_{\rm BV}-\frac{1}{2}T_{\rm BH}\right)=\frac{\partial(F_V-\frac{1}{2}F_H)}{\partial\theta}\Delta\theta \qquad (1).$$

A difference $\Delta\varphi=\varphi_{\rm true}-\varphi_{\rm rep}$ translates into an error of the third Stokes parameter and therefore into a along-scan bias of

$$\Delta U\approx-(V-H)\sin(2\Delta\varphi)\approx-2(V-H)\Delta\varphi \qquad (2)$$

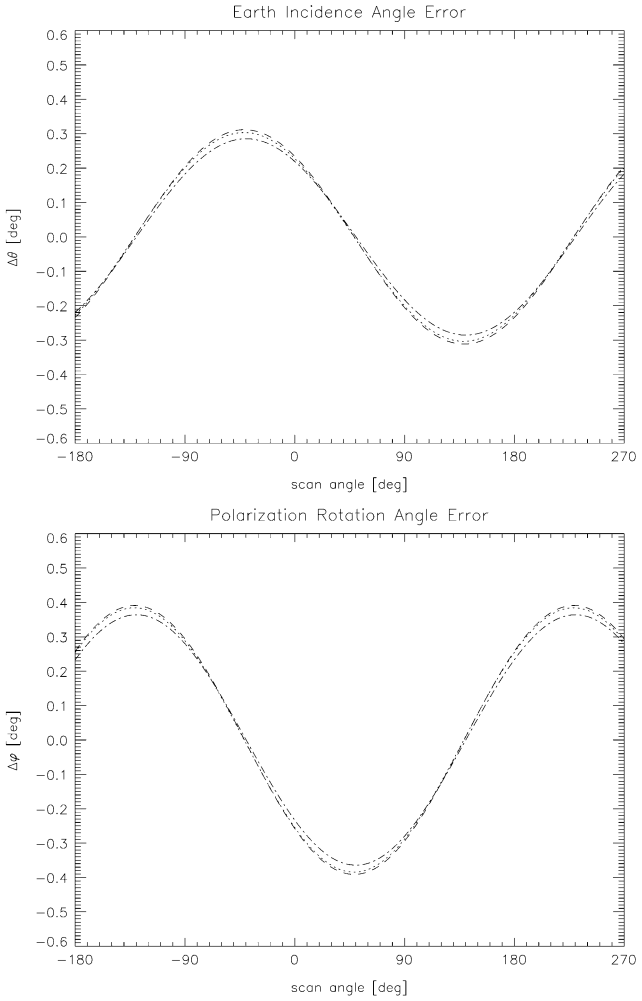

Fig. 6. Error in the EIA θ and the polarization rotation angle φ as function of the antenna boresight looking azimuth (scan angle) at (dotted line) 10.7, (dashed line) 18.7, and (dashed–dotted line) 37.0 GHz.

assuming that $\Delta\varphi$ is small and measured in radians. Using (1) and (2) we can easily calculate $\Delta\theta$ and $\Delta\varphi$ from the corresponding values for $\Delta(T_{\rm BV} - (1/2)T_{\rm BH})$ and ΔU from Fig. 5. In doing that we have subtracted the overall biases A_0 and inserted values for $\partial F/\partial\theta$ and $V - (1/2)H$ that were computed from the RTM for typical ocean–atmosphere scenes. The result is shown in Fig. 6. The most important feature is the fact the curves are almost identical for all three polarimetric bands. That means that the along-scan biases can be explained by an error in the EIA and an error in the polarization rotation angle that is phase shifted by 90° relative to the EIA error. Both errors are the same for all three polarimetric bands. Though not shown, this is also true for the two nonpolarimetric bands as far as EIA is concerned. The results for $\Delta\theta$ and $\Delta\varphi$ in Fig. 6 can be fitted by

$$\Delta\theta = \Delta\theta_o \sin(\omega - \omega_0)$$
$$\Delta\varphi = \Delta\varphi_o \sin\left(\omega - \omega_0 + \frac{\pi}{2}\right) \tag{3}$$

with $\Delta\theta_0 = 0.326°, \Delta\varphi_0 = 0.344°$, and $\omega_0 = -130.5°$.

3) Roll and Pitch Correction: The most likely explanation for the errors $\Delta\theta$ and $\Delta\varphi$ is a knowledge error in the S/C roll and pitch that were used to calculate the viewing geometry. It is not difficult to show that an S/C roll of $-0.159°$ and an S/C pitch of $+0.185°$ would produce an oscillation in θ and φ very similar to that shown in Fig. 6. For a final check, we subtracted $0.159°$ from the reported S/C roll angle and added $0.185°$ to the S/C pitch angle. These offsets are assumed to be constant over the entire time period considered herein. The above along-scan bias analysis was then repeated. The results are shown in the right panel of Fig. 5. It is clear that all the along-scan biases have basically vanished. It was very satisfying to see that the along-scan errors in all 22 WindSat channels were corrected by making a small change to the S/C roll and pitch.

The effect of this S/C roll and pitch correction to geographic contours, such as coastlines, can be easily seen from the equation for $\Delta\theta = \theta_{\rm true} - \theta_{\rm rep}$ in (3). The EIA difference corresponds to a tilt of the S/C $\hat{Z}$ axis by about 0.24°.

$\Delta\varphi(\omega)$ reaches its largest positive value of $\Delta\theta_0 = 0.326°$ when the boresight looking azimuth angle reaches a value of $\omega = \omega_0 + (\pi/2) = -40.6°$. In other words, at $-40.5°$ our correction tilts the look direction up and away from the Earth by 0.326°. From our sign convention for ω (positive if looking left of forward, negative if looking right of forward), it follows, that for an ascending orbit the correction shifts coastlines to the north and east.

D. Third Increment: Incorporation of Scan Bias Results

The pitch and roll knowledge biases identified in the scan bias analysis correlated well with those from the coastline matchups. The magnitudes matched closely and the directions were the same for both pitch and roll. The pitch and roll bias values calculated in the scan bias were incorporated into the data processing and another round of coastline matchups were performed.

Fig. 7 shows that the geolocation errors are now nearly imperceptible as well as showing extremely low values for pitch, roll, and within scan average errors. There were, however, notable yaw/beam-azimuth biases of $-0.14°$ in the 23.8 channels and $-0.06°$ in the 37 channels. The fact that the beam-azimuth/yaw errors are not consistent across all channels indicates that they are confined to individual antenna beams and thus caused by beam azimuth biases as opposed to systematic yaw errors. It was previously difficult to identify these errors from inside the roll/yaw/within-scan ambiguity, although, in hindsight, there were indications of this error source in the increment 2 data. The correct removal of the roll and pitch biases made these beam azimuth errors stand out clearly. It is important to note that both beam azimuth errors and yaw errors affect only geolocation; neither has any other effect on the wind retrieval.

These beam azimuth biases created typical geolocation errors of 2–3 km for the 23 channel and 1–2 km for the 37 channel. These subpixel geolocation errors were usually discernable in the temperature gradient maxima imagery and the averaging of several datasets provided the necessary accuracy to remove them.

E. Fourth Increment: All Errors Removed

The beam azimuth errors for the 23 and 37 channels were removed for the fourth increment. The possible .03° error in

THIRD INCREMENT: PITCH & ROLL BIASES FIXED				
	AVG PITCH (deg)	AVG ROLL (deg)	AVG WITHIN SCAN (uSEC)	AVG YAW / BEAM AZIMUTH (DEG)
10.7	0.00	0.01	-0.02	-0.01
18.7	0.00	0.01	-0.02	-0.03
23.8	0.00	0.00	0.00	-0.14
37	0.00	0.01	-0.02	-0.06
4 CHANNEL AVERAGE	**0.00**	**0.01**	**-0.02**	**-0.06**
ERROR DIAGNOSIS	ALL CHANNELS WELL INSIDE ERROR BUDGET AFTER PITCH AND ROLL ADJUSTMENTS			BEAM AZ ERRORS FOR 23, 37, 18?

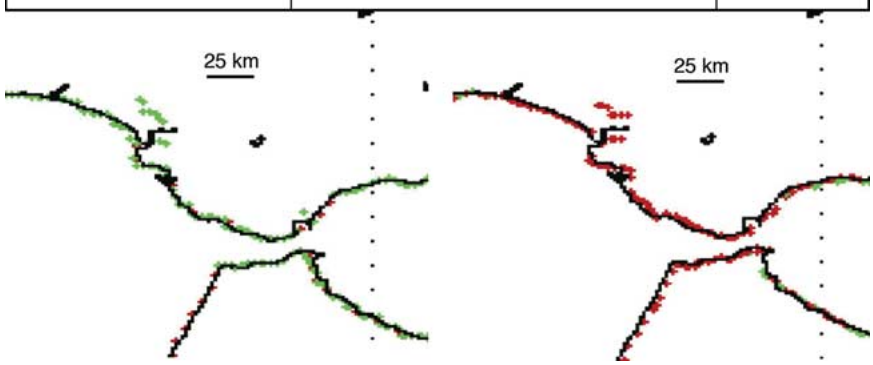

Fig. 7. Geolocation performance in third increment. The table summarizes the average error for several datasets taken from various geographic locations with various pass geometries. The images show a close-up image of local maxima in an area slightly smaller than 3° latitude × 3° longitude. The green dots in the local maxima plots represent cross-scan local maxima, while the red dots indicate along-scan local maxima. (Left) Forward scan. (Right) Aft scan.

the 18.7 channel was not removed because it was within error budget specifications and because the average of .03° resulted from barely discernable geolocation errors in only half the datasets. The removal of the errors was successful.

Overall, the WindSat geolocation errors were incrementally reduced to approximately 1 km or less and pointing errors were reduced to well within the error budget. Initial coastline matchup errors triggered an investigation that identified two time-tagging errors for correction but left ambiguous results showing possible roll and or pitch errors. The roll and pitch errors have a direct impact on the wind vector retrieval because of the induced cross-polarization. The scan bias analysis confirmed the error sources as roll and pitch biases, which were subsequently removed. The removal of the pitch and roll errors exposed beam azimuth biases in two bands. These were corrected eliminating any discernable geolocation errors. This process ultimately brought WindSat pointing knowledge and geolocation to within design tolerances and error budget specifications.

The coastline matchup and scan bias techniques are largely complementary tools for the correction of geolocation and pointing errors. The scan bias technique has the primary advantages of isolating pointing offsets and great accuracy available through averaging large quantities of data. The coastline matchup technique has strengths of quick outputs that show both pointing and timing errors. Additionally the coastline matchup technique quickly isolates consistent, bias, errors from inconsistent, random, errors. The WindSat experience was that the quick response of the matchup method removed the largest errors effectively enabling the scan bias method to resolve the smaller and more difficult pointing errors.

Confidence in the accuracy of the two methods was provided by their agreement in pointing and roll error magnitudes and directions (increment 2). Confidence in the precision available from the coastline matchups with the local maxima technique is provided by the excellent geolocation accuracy, particularly the near zero indicated roll and pitch errors, following removal of the pointing biases calculated by the scan bias analysis (increment 3).

IV. Conclusion

The WindSat pointing knowledge errors have been reduced to within error budget specifications of .05° and the geolocation accuracy is well below the required 5 km. Multiple errors were eliminated incrementally through a combination of coastline matchup geolocation analysis and scan bias analysis. These two methods provide a complementary means of identifying a wide variety of pointing and timing errors. The coastline method has fundamental pointing versus timing ambiguities and has limited subpixel resolution. The scan bias technique has accuracy inside 0.05° for pitch and roll errors. There was good agreement between the two methods on the magnitude and direction of the pitch and roll errors. Resolving the errors was greatly facilitated by open communication among the spacecraft, sensor, and ground software engineers.

APPENDIX
DEFINITIONS

A. Geolocation Errors

Geolocation Error: A mislocation of an imagery data sample's geographic location relative to where it should truly be located.

Cross Scan Geolocation Error: A geolocation error perpendicular to the direction of the scan path.

Along Scan Geolocation Error: A geolocation error along the direction of the scan path.

Forward and Aft Scan: The WindSat instrument gathers data from the forward direction and the aft direction relative to its flight path. These scans are labeled forward and aft, accordingly. The data are sequentially acquired starting at the beginning of each forward scan.

B. Pointing Errors

Pointing errors place data points at wrong geographic location in a manner characteristic of their cause.

Pitch Error: An error in the determination of the pitch angle of the instrument. These errors will move the imagery forward and aft along and parallel to the flight path for all channels equally.

Roll Error: An error in the determination of the roll angle of the instrument. These errors will move the imagery left and right perpendicular to the flight path for all channels equally.

Yaw Error: An error in the determination of the yaw angle of the rotating portion of the instrument. These errors will move the imagery along the scan for all channels equally.

Beam Elevation Error: An error in the determination of the elevation angle of the antenna beam. These errors will move the imagery perpendicular to the scan path for individual channels.

Beam Azimuth Error: An error in the determination of the azimuth angle of the antenna beam. These errors will move the imagery along to the scan path for individual channels. Azimuth errors have the exact same impact on geolocation and EDR retrievals as yaw errors. It is not necessary to distinguish between beam azimuth and yaw errors.

C. Timing Errors

Timing errors place data points at the wrong geographic location in a manner characteristic of their cause.

Systematic Timing Errors: Systematic timing errors apply equally to all data samples. These timing errors will move all imagery data samples forward or backward along and parallel to the flight path for all channels equally.

Within-Scan Timing Errors: The other major time error occurs in the within-scan time tagging. This error increases around the scan from the beginning of each forward scan until the end of each aft scan which is caused by a small error in the delta term in the timing equation

$$t_n = t_{\text{sync}} + n\Delta t$$

where

$$\begin{aligned} t_n &= \text{time of sample} n \\ t_{\text{sync}} &= \text{time stamp of the scan sync pulse} \\ \Delta t &= \text{the time between each sample} \end{aligned} \tag{A1}$$

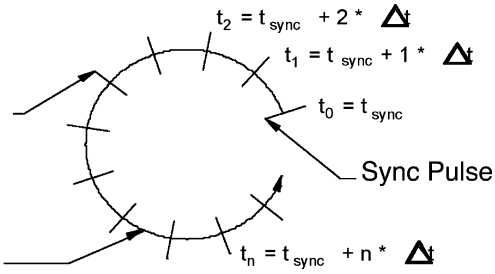

Fig. 8. Within-scan timing errors.

Fig. 8 shows a schematic of the time tagging within each scan. The synchronization pulse occurs at a fixed scan angle prior to the start of the forward scan. Each subsequent sample n is assigned a time t_n. Any error in Δt will shift imagery data samples along the scan with the size of the mislocation being proportional to n. These within scan timing errors will move imagery data samples along the scan with the amount of mislocation being proportional to the number of samples after the sync pulse. These errors appear as worsening geolocation around the scan.

REFERENCES

[1] P. W. Gaiser *et al.*, "The WindSat spaceborne polarimetric microwave radiometer: Sensor description and early orbit performance," *IEEE Trans. Geosci. Remote Sens.*, vol. 42, no. 11, pp. 2347–2361, Nov. 2004.

[2] G. A. Poe and R. W. Conway, "A study of the geolocation errors of the Special Sensor Microwave/Imager (SSM/I)," *IEEE Trans. Geosci. Remote Sens.*, vol. 28, no. 5, pp. 791–799, Sep. 1990.

[3] DMA, "Military specification: Digital landmass blanking (DLMB) data program," Defense Mapping Agency, Washington, DC, MIL-D-89021, Jun. 15, 1991.

[4] W. L. Lippincott, T. A. Gutwein, H. E. Bartlett, M. Smythers, P. W. Gaiser, and W. E. Purdy, "Antenna design, modeling and testing on the WindSat wind direction measurement system," Nav. Res. Lab., Washington, DC, Tech. Memo. Rep., Mar. 2002.

[5] G. A. Poe, E. A. Uliana, B. Gardiner, and T. von Rentzell, "Conical Microwave Imaging/Sounding: Geo-location error analysis," NPOESS Integrated Program Off., Washington, DC, NPOESS Int. Gov. Study, 2003.

[6] T. Meissner and F. Wentz, "Polarization rotation and the third Stokes parameter: The effects of spacecraft attitude and Faraday rotation," *IEEE Trans. Geosci. Remote Sens.*, vol. 44, no. 3, pp. 506–515, Mar. 2006.

[7] F. Wentz and T. Meissner, "AMSR ocean algorithm (Version 2) Algorithm Theoretical Basis Document (ATBD)," Remote Sens. Syst., Santa Rosa, CA, 2000.

[8] P. W. Gaiser, "WindSat TDR version 146AFBBDA," Nav. Res. Lab., Washington, DC, Data and Format Description, Dec. 2003.

William E. Purdy received the B.S. degree in mechanical engineering from the University of Maryland, College Park, in 1986.

He has specialized in spacecraft systems engineering and spacecraft mechanisms over an 18-year career including working at the Naval Research Laboratory from 1986 to 1999. He is currently the proprietor of Purdy Engineering, Poolesville, MD, from 1999 to present. He has performed as a Systems Engineer on the WindSat program with responsibilities for alignments, antenna systems engineering, and mechanical systems engineering. He has worked on 25 spacecraft in a wide variety of roles ranging from subsystem manager to program manager.

Peter W. Gaiser (S'91–M'93–SM'04) received the B.S. degree in electrical engineering from Virginia Polytechnic Institute and State University, Blacksburg, in 1987, and the Ph.D. degree from the University of Massachusetts, Amherst, in 1993, where he studied microwave remote sensing, with emphasis on synthetic aperture interferometric radiometry.

He has been with the Naval Research Laboratory (NRL), Washington, DC, since 1993, and currently Acting Head of the Remote Sensing Physics Branch, Remote Sensing Division at NRL. While at NRL, he has been involved in polarimetric radiometry research. His research interests also include instrument design, data collection, and model development specifically for the purpose of ocean wind vector measurements from space. He is the Principal Investigator for the WindSat spaceborne polarimetric microwave radiometer demonstration project.

Gene A. Poe (M'91) received the B.A. and M.S. degrees in electrical engineering from the University of California, Berkeley, in 1964 and 1965, respectively.

He has worked in wide-ranging companies responsible for the development of space-based passive microwave radiometer instruments (Aerojet Corporation: 1965–1972 and 1989–1993; Hughes Aircraft Company: 1976–1982). From 1986 to 1989 and from 1993 to the present, he has been with the Marine Meteorology Division, Naval Research Laboratory (NRL), Monterey, CA, as well as the NRL, Washington, DC facilities. He was Team Leader for the joint Air Force/Navy DMSP calibration/validation programs for the F-13 through F-15 SSM/I instruments and Core-Team Member of the WindSat calibration/validation program. Currentlym he is Technical Leader of the DMSP calibration/validation effort of the Special Sensor Microwave Imager/Sounder, SSMIS.

Mr. Poe is a member of the American Mathematical Society.

Enzo A. Uliana, photograph and biography not available at the time of publication.

Thomas Meissner received the B.S. degree in physics from the University of Erlangen-Nürnberg, Nürnberg, Germany, the M.S. degree (Diploma) in physics from the University of Bonn, Bonn, Germany, and the Ph.D. degree in theoretical physics from the University of Bochum, Bochum, Germany, in 1983, 1987, and 1991, respectively. He wrote his doctoral dissertation on effective quark models of the nucleon.

Between 1992 and 1998, he conducted postdoctoral research at the University of Washington, Seattle, the University of South Carolina, Columbia, and Carnegie Mellon University, Pittsburgh, PA, in theoretical nuclear and particle physics, focusing on the theory of strong interaction. Since July 1998, he has been with Remote Sensing Systems, Santa Rosa, CA. Since then, he has been working on the development and refinement of radiative transfer models, calibration, validation, and ocean retrieval algorithms for various microwave instruments (SSM/I, TMI, AMSR-E, WindSat, CMIS).

Frank J. Wentz received the B.S. and M.S. degree in physics from Massachusetts Institute of Technology, Cambridge, MA, in 1969 and 1971, respectively.

In 1974, he established Remote Sensing Systems (RSS), Santa Rosa, CA, a research company specializing in satellite microwave remote sensing of the Earth. His research focuses on radiative transfer models that relate satellite observations to geophysical parameters, with the objective of providing reliable geophysical datasets to the Earth Science community. As a member of the National Aeronautics and Space Administration's (NASA) SeaSat Experiment Team (1978–1982), he pioneered the development of physically based retrieval methods for microwave scatterometers and radiometers. Starting in 1987, he took the lead on providing the world-wide research community with high-quality ocean products derived from satellite microwave imagers (SSM/I). As the Director of RSS, he overseas the production and validation of reliable scatterometer and radiometer products. These data are dispersed via the company's web and ftp sites. He is currently a member of NASA Earth Observation System Investigators Working Group, NASA Advanced Microwave Scanning Radiometer Team, NASA Ocean Vector Wind Science Team, NASA Tropical Rainfall Mission Team, and NASA Pathfinder Activity. He is currently working on scatterometer/radiometer combinations, satellite-derived decadal time series of atmospheric moisture and temperature, the measurement of sea-surface temperature through clouds, and advanced microwave sensor designs for climatological studies

Mr. Wentz has served on many NASA review panels, the National Research Council's Earth Studies Board, the National Research Council's Panel on Reconciling Temperature Observations, and is a member of the American Geophysical Union.